Microscopic analysis of the water/glycerol/EO30PS system in bulk and on a solid substrate

Makoto Uyama, Roland Steitz, Marcus Trapp, Laurence Noirez, Sebastian Bayer, Michael Gradzielski

Microscopic analysis of the water/glycerol/EO30PS system in bulk and on a solid substrate

Makoto Uyama,*,† Roland Steitz,*,‖ Marcus Trapp,‖ Laurence Noirez,‡ Sebastian Bayer,§ and Michael Gradzielski*,§

†Shiseido Co., Ltd. MIRAI Technology Institute, Kanagawa 220-0011, Japan,

‖Helmholtz-Zentrum Berlin für Materialien und Energie GmbH, Hahn-Meitner-Platz 1 14109 Berlin, Germany

‡Laboratoire Léon Brillouin CEA-CNRS, Université Paris-Saclay, CEA Saclay, 91191 Gif sur Yvette Cedex, France

§Stranski-Laboratorium für Physikalische und Theoretische Chemie, Institut für Chemie, Technische Universität Berlin, Strasse des 17 Juni 124, Sekr. TC7, 10623 Berlin, Germany

*Corresponding authors: M.U.: makoto.uyama@shiseido.com

R.S.: steitz@helmholtz-berlin.de

M.G.: michael.gradzielski@tu-berlin.de

ABSTRACT: Surfactant systems are often employed in cosmetic formulations where they dry on skin as a surface, thereby becoming increasingly concentrated systems. In order to better understand this drying process we focused on the difference of self-assembled structures of water/glycerol/polyoxyethylene (30) phytosteryl ether (EO30PS) system in bulk and on a solid substrate, because the interaction between substrate and surfactant has a substantial effect on the self-assembly, which may be related to the bulk structure but in detail may also differ strongly from the bulk situation. In bulk, small neutron angle scattering (SANS) experiments showed that with increasing loss of water, the degree of ordering increases but changes of the aggregate structure are rather small. The results indicate that ellipsoidal micelles of EO30PS are densely packed and simply become more ordered in bulk during the drying process. On the other hand, neutron reflectometry (NR) revealed that EO30PS molecules adsorb onto a Si surface in form of bilayers and analysis indicates that at high concentration (c = 20 wt%) there are on average two bilayers (a double bilayer) on the SI substrate. The adsorbed membrane structure of EO30PS is rather thin with respect to its hydrophobic part, indicating tilted molecules, containing only some solvent, and being not highly ordered. These experimental results then allow for a much deeper understanding of the structural properties of practical formulations as they are applied for instance in cosmetic lotions.

INTRODUCTION

In pharmaceutical, cosmetics, detergency, and painting applications,[1,2,3] it is very important to understand the structural changes that occur during the drying process of formulations, as from a physico-chemical point of view that is essentially happening during their practical application (mainly evaporation of water). During the drying process, one has an increasing concentration of surfactant, polymer and oil in a water-based formulation.[4] Of course, for the understanding of the practical performance of such systems it is of central importance to have complete knowledge of how their structure changes during this evaporation process. Typically, such lotions are supposed to deliver

active agents to their substrate during drying, and, of course, any transport process in this application is controlled by the bulk structures present and even more by the interfacial structures, especially for transdermal transport. Naturally, during the concentration process liquid crystalline phases or other ordered structures are likely to be formed. They may vary quite differently with respect to their detailed structure depending on the precise composition of the formulation, i.e., on the type of surfactant and polymer contained. From phase studies and light scattering one can get some insights into the changes taking place in such systems, but as they are multicomponent systems for further reaching structural information on the bulk structure one may require small-angle neutron or x-ray scattering (SANS, SAXS). However, SAXS typically suffers from poor contrast conditions and, in addition, quite substantial radiation damage may occur, especially for polymers. Therefore, SANS is ideally suited to gain information regarding the mesoscopic structures in the size range of 1-200 nm, as relevant in these mixed amphiphilic systems in order to derive a systematic understanding of the relation between the composition of the formulation and its performance in application, where we were in particular interested in applications on skin. Of course, skin is a very complex interface and for a good fundamental understanding one may first turn to simple model interfaces.

It is also very important to understand the static and dynamic adsorption processes of surfactants on a substrate and the structure of the adsorbed dried film, as that are key factors that control function and properties of the formed film.[4,5] For these processes the interaction between substrate and surfactant has a substantial effect on the self-assembly, which may be related to the bulk structure, but in detail may also differ strongly from the bulk situation. Therefore, information about the bulk aggregation structure is insufficient to gain the required insights into the prevailing interfacial structure. In our study we were interested in the structure of the adsorbed layer on the substrate (here hydrophilic Si to mimic skin, which is our ultimate interest) when we put solutions of surfactant/glycerol/water with variable concentration on it. Hydrophilic Si will be more hydrophilic than real skin and therefore is not a perfect model system, but has the advantage of being available with a very well-defined and smooth surface, which is essential for good reflectometry experiments.

For further experiments it could certainly be interesting to employ more realistic materials as substrate where the challenge will be to have them as smooth as possible.

The adsorbed layer can be studied by QCM (Quartz Crystal Microbalance) or ellipsometry, which yield information on the adsorbed amount or thickness, however, without yielding information about its mesoscopic structure. X-ray reflectometry depends on the atomic number and therefore the method is similar to SAXS limited in yielding information on surfactant/glycerol/water based layers, as the contrast conditions here are difficult to interpret. Therefore, neutron reflectometry (NR) measurements were done to complete the above mentioned experiments. NR provides unique structural information on such layers, for instance the structure and thickness of the adsorbed layer,[6] as by using D_2O (or further selective deuteration schemes) one can control the contrast conditions and deduce detailed information on the layer structure. In addition, one can address the question of the penetration of the solvent into the layer. Such experiments allow to deduce relationships between the way of adsorption and the final structure after bulk water is evaporated and to deduce in which ways the self-assembly at the substrate surface relates to the bulk structures.

Accordingly, we did such experiments with a model lotion of surfactant/glycerol/water and studied the concentration dependence of its structure in the bulk and at the interface, where ultimately we would be interested in skin, but which for these experiments we substituted it by hydrophilic silica, which has the required smoothness for the reflectivity experiments. Based on that information we will gain a comprehensive understanding of the structural changes during the evaporation process and of the static and dynamic adsorption process of surfactants on a substrate. Comparison to the observed performance of such cosmetic lotions in practical applications shall help to develop a comprehensive understanding of how its molecular composition controls the mesoscopic structure during the evaporation process in bulk and the interface and how this then in turn determines the cosmetic performance.

EXPERIMENTAL SECTION

Materials. For all experiments, except neutron scattering, deionized MilliQ water (> 18.2 MΩ cm^{-1}) was used. D_2O (> 99.8 %) and glycerol-d8 employed in the neutron scattering experiments were purchased from Sigma-Aldrich (Missouri, USA). Polyoxyethylene (30) phytosteryl ether (EO30PS) (as shown in Figure 1; M_w = 1736 g/mol) was supplied by Nihon Surfactants Kogyo (Tokyo, Japan). Glycerol was purchased from Fujifilm Wako Pure Chemical Corporation (Osaka, Japan). All chemical materials were used as received.

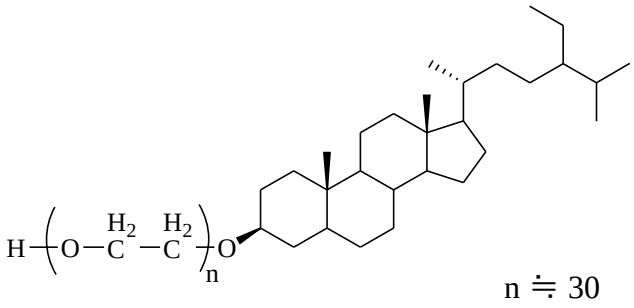

Figure 1. The chemical structure of EO30PS

Prepared samples are always described in terms of mass ratios for H_2O/glycerol/EO30PS (the concentrations are given in wt%, e.g., 48/32/20), where for the case of using D_2O (neutron experiments) this was recalculated in terms of the corresponding H_2O sample, i.e. they then possess an identical molecular composition.

Dynamic Light Scattering (DLS) measurements DLS measurements were performed at 20 °C using an ALV/CGS-3 instrument, equipped with a He−Ne laser with a wavelength of 632.8 nm. Pseudo-cross-correlation functions were recorded using an ALV 5000/E multiple-τ correlator at eleven scattering angles θ (10° apart) in the range 40−140° with an ALV-SP 125 goniometer. Cylindrical sample cells were placed in an index matching vat filled with toluene (±0.1 °C). The scattering angle θ defines the magnitude (q) of the scattering vector: $q = 4\pi n \sin(\theta/2)/\lambda$, with n being the refractive index of the solution, and λ the incident wavelength of light. The intensity autocorrelation function $g^{(2)}(\tau)$ was obtained by averaging the results of three repeat measurements,

and then converted to the field autocorrelation function $g^{(1)}(\tau)$ by the Siegert relation:[7,8]

$$g^{(2)}(\tau) = 1 + B|g^{(1)}(\tau)|^2 \quad (1)$$

For monodisperse samples $g^{(1)}(\tau)$ relaxes by simple exponential function as described by: $g^{(1)}(\tau) = \exp(-\Gamma\tau)$, where Γ is the relaxation rate. For diffusive relaxation Γ is given by: $\Gamma = q^2D$, where D is the translational diffusion coefficient. In this study, hydrodynamic radii and polydispersity index were calculated by using a cumulant analysis method. The curves were fitted to the cumulant expansion (eq. 2) for obtaining decay rates at each angle. In the cumulant method, the logarithm of $g^{(1)}(\tau)$ is expanded with regard to cumulants of the distribution.[9]

$$\ln\left[g^{(1)}(\tau)\right] = -\Gamma\tau + \frac{1}{2}\mu_2\tau^2 - \frac{1}{6}\mu_3\tau^3 \quad (2)$$

Diffusion coefficients D were obtained from the slope of the Γ versus q^2 plots. The hydrodynamic radius (R_h) was determined by the Stokes-Einstein equation: $R_h = k_BT/6\pi\eta D$, where T is temperature, k_B Boltzmann's constant, and η viscosity of solvent. From the cumulant analysis, a polydispersity index (PDI) was calculated according to: PDI = μ_2/Γ^2.

Small Angle X-ray Scattering (SAXS) measurements SAXS measurements were performed with a SAXSess camera (Anton Paar). Cu-Kα (λ: 1.542 Å) radiation was used. The scattering intensity of each sample was measured at 25 °C for 10 min with a cyclone imaging plate detection system (Perkin-Elmer, Waltham, MA, USA) and analyzed by SAXSQuant software (Anton Paar).

Small Angle Neutron Scattering (SANS) measurements SANS was performed at the instrument PAXY of the Laboratoire Léon Brillouin (LLB, CEA-CNRS, Saclay, France) with a neutron wavelength of 6 Å, a sample-to-detector distance of 3 m, and a collimation of 3 m. The covered range of the magnitude of the scattering vector was $0.08 < q < 1.3$ nm^{-1}. Empty cuvette and cuvette with D_2O were used to subtract the sample background. Distillated water was used as incoherent scatterer to calibrate the detector efficiency, and the attenuated direct beam was used to determine the absolute scaling.[10,11] The data reduction and radial average was done with the software BerSANS[12] in order to obtain the absolute scattered intensity as a function of the magnitude, q, of the scattering vector. The solvent was D_2O in order to reduce the incoherent background and increase the contrast. Quartz cells

(Hellma 110-QS) of 1 mm thickness were used for all measurements. Measurements were done at 25 °C.

Neutron Reflectometry (NR) measurements NR experiments were performed at the Helmholtz-Zentrum Berlin (Berlin, Germany), using the instrument V6.[6,13-15] The incident neutron beam had a wavelength λ =4.66 Å and a rectangular cross section (0.5 mm x 40 mm), passed through the silicon block and was reflected off the silicon/liquid interface, and subsequently counted with a ^{3}He detector. The reflectivity was measured as a function of the reflection angle θ. The measurements were performed in a $\theta/2\theta$ geometry (detector angle) from q = 0.0028 to 0.10 Å^{-1}. Scans were recorded with sampling times per step from 7.0x10^4 monitor counts for 0.0028 Å^{-1} to 0.033 Å^{-1}, 2.1x10^5 monitor counts for 0.033 Å^{-1} to 0.0056 Å^{-1}, 8.5x10^5 monitor counts for 0.0056 Å^{-1} to 0.075 Å^{-1}, and to 1.6x10^6 monitor counts for 0.075 Å^{-1} to 0.10 Å^{-1}. Data points were obtained at θ = 0.020º intervals for 0.033 ≤ q ≤ 0.075 Å^{-1} and θ = 0.030º intervals for 0.075 ≤ q ≤ 0.10 Å^{-1}. The data sets were normalized with respect to monitor counts and incident intensity. Reflected intensities, I, were normalized to the number of incoming neutrons, I_0, which yields the neutron reflectivity, $R = I/I_0$. The data were obtained as a function of momentum transfer q (or magnitude of the scattering vector). A homemade sample cell for the neutron reflectivity studies was adopted as reported previously.[16] The sample cell was filled with sample solution and was equilibrated for at least 0.5 h prior to starting the experiment. As substrate, silicon blocks of n-type were used, with dimensions 80 mm × 50 mm × 15 mm (Siliciumbearbeitung Andrea Holm GmbH, Tann, Germany). Before measurements, the polished surface of a silicon block was cleaned using the RCA method to make the surface hydrophilic.[17] Data fitting was carried out using Motofit for Igor Pro 7.[18,19]

RESULTS and DISCUSSIONS

In the bulk system

As a first step, we studied the given system in the bulk state at different concentrations since one may expect that the main difference that arises during drying is simply the changing concentration in the system and concomitant changes of the bulk structure.

Bulk phase behavior

A first important insight into the systems can be obtained by determining the macroscopic phase behavior. Figure 2 shows the triangle phase diagram of water/glycerol/ EO30PS system at 25 °C. Phase state determination was performed by direct visual inspection and observation with crossed polarizers. In the area rich of water, normal discontinuous micellar cubic (I_1) and normal hexagonal (H_1) phases can be seen (in agreement with a previous study[20]), while the aqueous micellar solution (L_1) dominates large areas. In contrast, EO30PS was found to be largely insoluble in glycerol. For less than 20 wt% water, hydrated crystals (S) of EO30PS were observed.

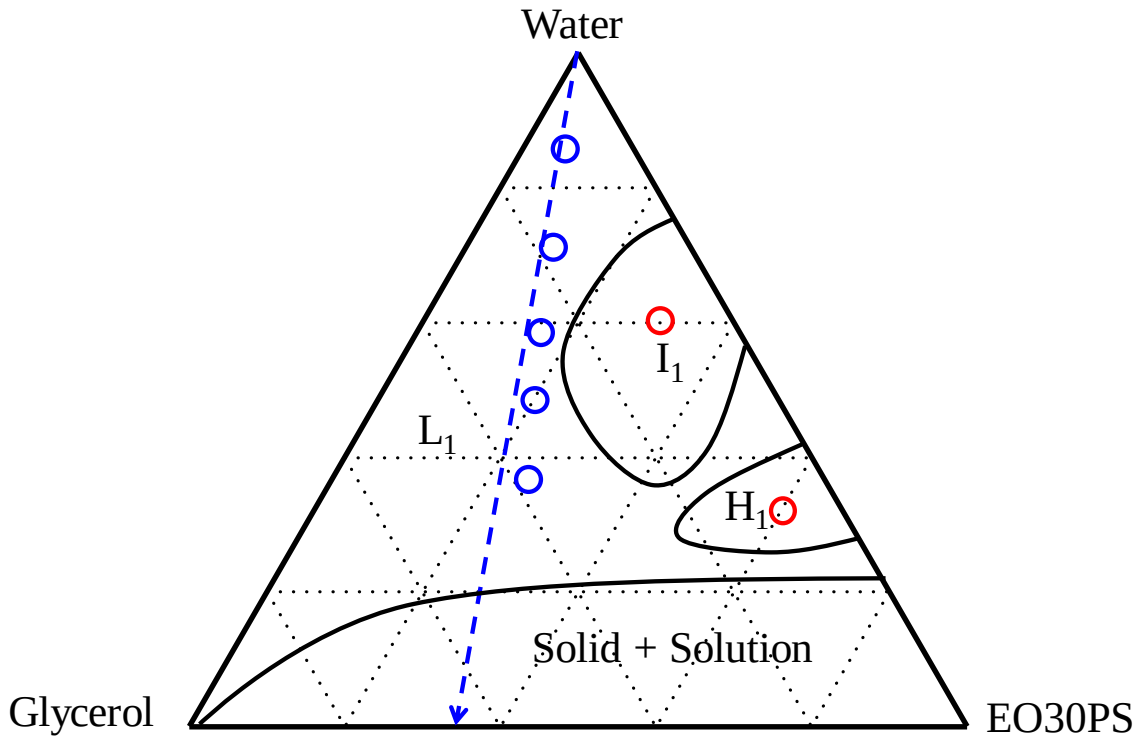

Figure 2. Phase diagram of water/glycerol/EO30PS system at 25 ºC. The phases shown are the aqueous micellar solution (L_1), normal discontinuous micellar cubic (I_1), and normal hexagonal (H_1) phases. Open red circles show the measured samples for SAXS. Dashed blue arrow shows the dilution

line. The I_1 + H_1 indicates a coexistence of I_1 and H_1 phases. Open blue circles show the measured samples for DLS, SANS, and NR.

The SAXS pattern of water/glycerol/EO30PS = 30/10/60 system is shown in Figure 3 (a) and the diffraction pattern suggests the presence of a normal hexagonal (H_1) phase. From the peak position, we calculated the lattice constant as 9.2 nm, and here cylindrical aggregates should be present. The existence of an H_1 phase of water/glycerol/EO30PS = 30/10/60 system was further confirmed by polarized light microscopy which showed a fan-like texture typical for hexagonal phases (image shown in the SI, Figure S1). The SAXS pattern of the water/glycerol/EO30PS = 60/10/30 system is shown in Figure 3 (b). We confirmed that the system is an isotropic phase by polarized light microscopy observation (image shown in the Figures S1, S2) and the sample of this system produced a ringing sound when tapped with a hard object. Such ringing properties are often associated with the presence of a cubic phase[21], which may be continuous[22] or discontinuous[23] in structure. From the location in the phase diagram (being between the L_1 and the H_1 phase), we identified this phase as normal micellar cubic phase I_1. From the diffraction peaks it was concluded to be a fcc (face centered cubic) lattice and the lattice constant was calculated as 20.2 nm. Assuming this to be the size of a normal fcc elementary cell and accounting for the surfactant concentration of the sample (using the densities given in Table S1) we arrive at an average aggregation number of 226 for a single micellar aggregate, which is in good agreement with the size determined by light and neutron scattering (discussed in the following). It should be noted here that Folmer et al.[20], Naito et al.[24], and Teshigwara et al.[25] have studied the phase diagrams of several phytosterol ethoxylate surfactants and our results are consistent with their results.

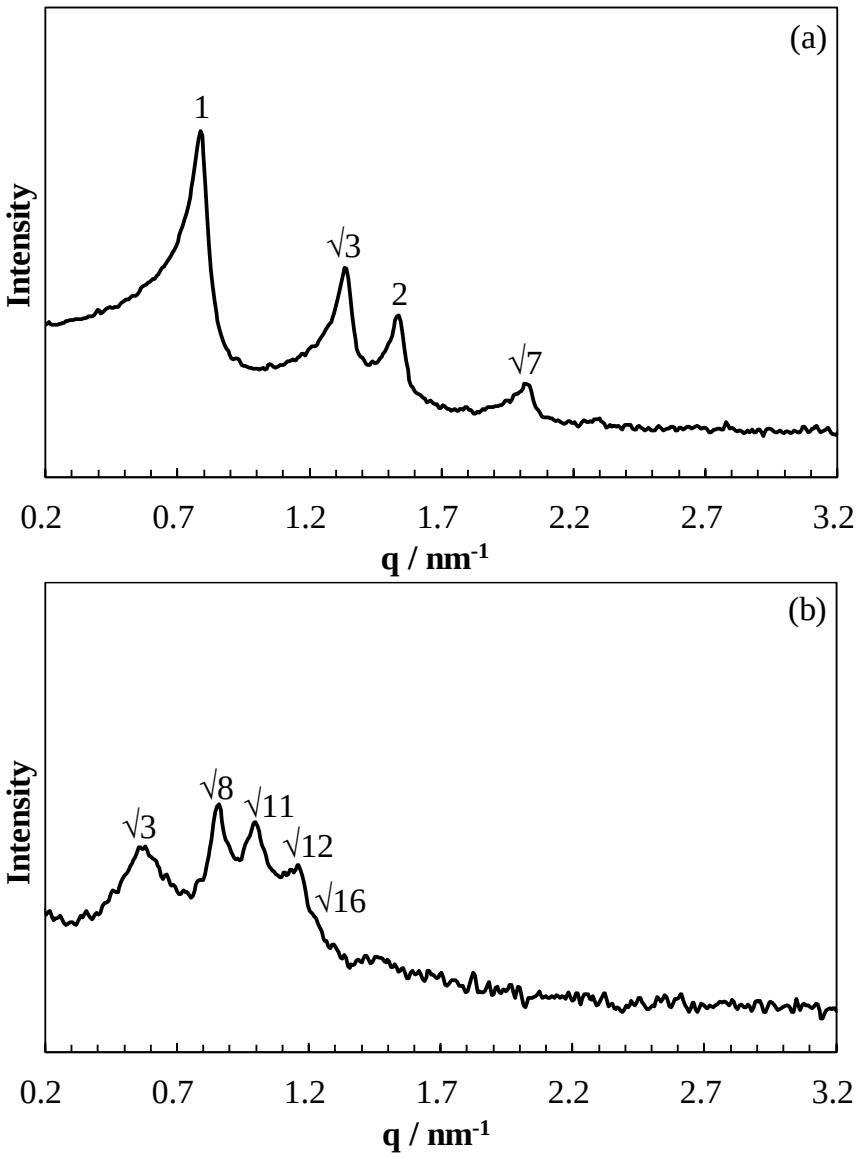

Figure 3. SAXS patterns of (a) water/glycerol/EO30PS = 30/10/60, (b) water/glycerol/EO30PS = 60/10/30 systems.

DLS measurements

DLS measurements have been done with the samples on the dilution line shown in Figure 2 (blue dashed line) reflecting the actual drying process (loss of water at constant glycerol/surfactant ratio) and for a series with a constant 5 wt% EO30PS and varying the solvent composition from pure water to a 70/30 glycerol/water mixture (in Table 1). The samples along the dilution line were having the composition: water/glycerol/EO30PS = 85.5/9.5/5, 72/18/10, 59.5/25.5/15, 48/32/20, 37.5/37.5/25 (by weight), thereby increasing the relative concentration of glycerol in the solvent from 10 to 50 wt%. As one can see from the autocorrelation functions and cumulant fitting of the curves shown in

Figure 4, samples for water/glycerol/EO30PS = 48/32/20 and 37.5/37.5/25 systems show a tailing second mode, potentially arising from collective relaxation in these much more viscous samples, where the viscosity can simply be attributed to the high concentration. In contrast, the monomodal decays for the water/glycerol/EO30PS = 85.5/9.5/5, 72/18/10, and 59.5.5/25.5/15 systems indicate that the aggregates are rather monodisperse (more cumulant fitting curves at different angles as well as for the different systems are shown in Figures S3-S11). From the fits, we calculated the hydrodynamic radius R_h, translational diffusion coefficient D, and polydispersity index PDI, by using the data of refractive index and viscosity of the water-glycerol mixture[26-28] and these parameters are shown in Table 1 (it might be noted that the very high PDI values for samples with 20 and 25 wt% EO30PS are unrealistic and should be the result that at such high concentrations one does no longer observe simple diffusion of the micelles). With increasing EO30 PS concentration the apparent hydrodynamic radius R_h becomes smaller, which can be attributed to the fact that here we look at very concentrated systems, where the repulsive interactions are becoming stronger, resulting in a lower structure factor at low q (as seen in the SANS experiments, Figure 5). According to the relation: $D(q) = D_0/S(q) \sim 1/R_h$, a reduced value of R_h will be observed. Accordingly, these values become increasingly less reflecting the real size of the aggregates contained. In addition, by the largely increasing values of PDI we see that the autocorrelation functions no longer follow a simple relaxation pattern, but apparently the strong interactions present widen the relaxation process largely.

In contrast, the series with constant concentration of 5 wt% EO30PS is much easier to interpret. With increasing relative glycerol concentration, R_h becomes smaller. This can be explained by a desolvation of the polyoxyethylene block due to its lower affinity to glycerol (as seen in the fact that EO30PS is not soluble in pure glycerol), which then results in a reduced extension of the EO30 head group into the solvent. The more collapsed EO block then has a larger head group area requirement, thereby leading to smaller micelles.

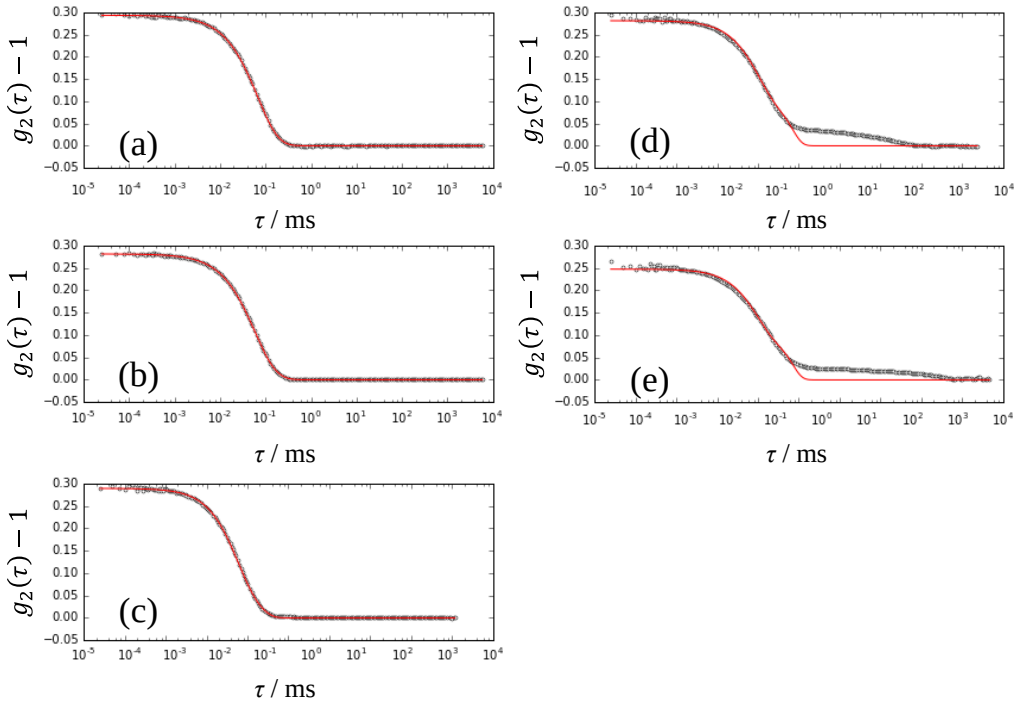

Figure 4. Autocorrelation functions (black lines) and cumulant fitting curves (red lines) at scattering angle 70° obtained from water/glycerol/EO30PS = (a) 85.5/9.5/5, (b) 72/18/10, (c) 59.5/25.5/15, (d) 48/32/20, and (e) 37.5/37.5/25. The measurement time was (a), (b), and (c) 30s, (d) and (e) 240 s (T = 20 °C).

Table 1. Hydrodynamic radius (R_h), translational diffusion coefficient (D), and polydispersity index (PDI) for water/glycerol/EO30PS system.

Sample	R_h / nm	D / μm^2/s	PDI
water/EO30PS = 95/5	5.28	40.6	0.0393
water/glycerol/EO30PS = 85.5/9.5/5	5.34	30.7	0.0664
water/glycerol/EO30PS = 66.5/28.5/5	4.89	17.6	0.113
water/glycerol/EO30PS = 47.5/47.5/5	4.61	7.75	0.158
water/glycerol/EO30PS = 28.5/66.5/5	4.17	2.29	0.168
water/glycerol/EO30PS = 72/18/10	4.33	28.1	0.143
water/glycerol/EO30PS = 59.5/25.5/15	3.31	25.9	0.373
water/glycerol/EO30PS = 48/32/20	4.17	13.8	0.873
water/glycerol/EO30PS = 37.5/37.5/25	2.93	12.2	1.11

SANS studies

In addition to the DLS studies, more detailed information on the structural changes of the aggregates

that occur during the drying process on the mesoscopic length scale of 1-50 nm was obtained from SANS experiments. Sample compositions were the same as those in DLS measurements shown in Figure 4. Different from the DLS measurements we used D_2O for SANS measurements but kept the molar ratios fixed (thereby accounting for the density difference of H_2O and D_2O). As shown in Figure 5, with increasing loss of water one sees the expected marked increase of the correlation peak and thereby of the degree of ordering and only rather small changes of the aggregate structure (as the shape of the scattering curves at high q changes only little).

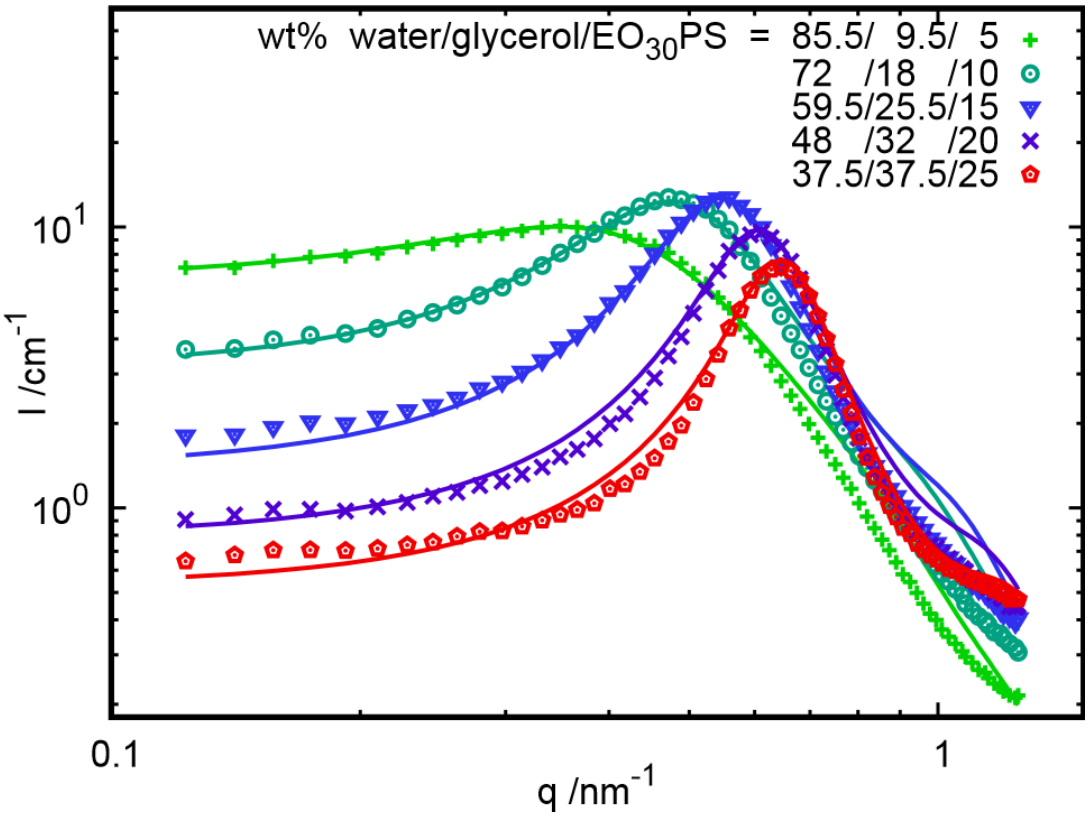

Figure 5. SANS intensity $I(q)$ as a function of the magnitude q of the scattering vector at 25 ºC for the D_2O/glycerol/EO30PS = 85.5/9.5/5, 72/18/10, 59.5/25.5/15, 48/32/20, and 37.5/37.5/25 (symbols explained in the inset indicate the sample composition, which is based on that of a corresponding H_2O sample). Solid lines are the fits from a model with monodisperse ellipsoidal form factor with hard sphere structure factor vs q.

The mean spacing d between aggregates was calculated from the peak position ($d = 2\pi/q_{max}$) and can serve for a first determination of the micellar size. For this the volume fraction of the micelle core (φ_{core}) was estimated by assuming the density of EO30PS as 1.03 g/cm^3 and the molecular weight of

hydrophilic and hydrophobic parts as 1337 and 399 g/mol, respectively. Assuming a primitive cubic arrangement from the mean spacing and taking the φ_{core} values, the radius of the micelle core (R_{core}) would be between 2.30 and 2.50 nm for all systems. The phytosteryl group of the EO30PS has a similar length as the cholesterol molecule of about 1.6 nm.[29] Therefore if the micelle would be truly spherical, then R_{core} should be around 1.6 nm. As the experimental values were larger than 1.6 nm, the EO30PS micelle must deviate from spherical shape. Folmer et al. determined the axial ratio of EO30PS micelle to be between 2.0 and 3.5, indicating that EO30PS micelle is not spherical but cylindrical.[20]

Table 2. Parameters obtained from the SANS analysis of the samples of different composition (described in detail in Tables S2 and S3): fraction of EO counted into the micellar aggregate x_{EO}, semi-major and semi-minor axis of the rotational ellipsoid R_e and R_p, factor x_{HS} by which the hard sphere volume is larger than that of the non-hydrated micelle (not accounting for the part 1-x_{EO} that is not considered to be part of the micelle), hard-sphere radius R_{HS}, mean spacing d, and aggregation number N_{agg}.

Sample	x_{EO}	R_e/nm	R_p/nm	x_{HS}	R_{HS}/nm	d/nm	N_{agg}
water/glycerol/EO30PS = 85.5/9.5/5	0.34	5.0	2.3	5.05	6.6	21.8	185
water/glycerol/EO30PS = 72/18/10	0.35	4.6	2.1	4.95	6.0	15.6	137
water/glycerol/EO30PS = 59.5/25.5/15	0.30	4.3	2.0	4.85	5.6	13.2	127
water/glycerol/EO30PS = 48/32/20	0.24	4.2	1.8	4.40	5.2	11.7	123
water/glycerol/EO30PS = 37.5/37.5/25	0.22	4.4	1.7	3.85	5.0	11.0	127

Therefore, we applied a core-shell ellipsoidal model for our systems and the detailed analysis of the SANS data on absolute scale was done by this model for the micelles that interact via a hard-sphere potential. Details are described in the supporting information. The result of this analysis is summarized in Table 2 and one finds that the aggregation number is almost constant and in the range of 125-140 for all samples except the most diluted one, for which a somewhat higher number has been deduced. The presence of elongated ellipsoidal micelles might be favored for the more dilute case of 5 wt% EO30PS and then upon further concentration the micelles will effectively overlap and apparently this repulsion then results in less elongation and formation of more spherical micelles, in order to reduce repulsive interactions. It should be noted that this model is in good agreement with

the simplified model described before in which the micellar size was simply deduced from the position of the correlation peak. As a result, the aggregation number decreases somewhat with increasing concentration, in a similar fashion as observed in DLS (Table 1). At the same time, the hard sphere interaction radius decreases with decreasing water content, which points to a compaction of the aggregates due to the increasingly crowded environment. This can be related directly to the fact that glycerol is apparently not interacting favorably with the EO head groups (as the EO30PS is also not soluble in glycerol, see Figure 2), and by reducing the water content in the solvent mixture one is reducing their solvation. Iwanaga et al. investigated the effect of polyols on the self-assembled structures of polyoxyethylene (7) lauryl ether and revealed that the two phase separation region is expanded by the addition of glycerol.[30] Our obtained results are in good agreement with their conclusions. At the highest concentration the distance from the micellar surface (where the EO part leaves the core of the micelle) to the neighboring micellar surface is ~ 6 nm, which means that here the EO_{30} chains have to overlap substantially, thereby reducing the observed value for R_{HS}. The best fit was obtained for an oblate ellipsoidal shape (the corresponding fitted data are shown in Figure 5) with the polar axis being half the length of the equatorial axes, i.e., having an axial ratio of two. However, it should be noted that a better fit quality by an oblate model is often observed for non-spherical micelles and does not necessarily exclude a prolate shape. Actually, the deviations at lower q (especially for the more concentrated samples) even indicate that the aggregates might actually be more elongated, but this could also be attributed to a less repulsive interaction as described by a hard sphere model (the overlapping EO head groups of different micelles should effectively introduce some attractiveness). In addition, we worked here with a monodisperse hard sphere structure factor, while in reality polydispersity of the micelles will be present and this also leads to an increase of the scattering intensity at lower q, as it is experimentally observed by us. In summary, we belief that polydispersity and an attractive component in the interaction potential are responsible for differences seen at low q between the experimental data and the fitted curves.

The observed deviations at $q > 0.8$ nm^{-1} can be attributed to the simplified model in which we assume

a step-wise contrast between the micelles and their surrounding medium. Realistically this cannot be the case as the segment density of the EO units will decrease continuously and in addition, at high q the scattering of the individual chains will start to contribute. However, these aspects were not fundamental/crucial for the present analysis, where we mainly focused on the aggregation number and shape of the micelles, which is soundly deduced.

On the surface of the silicon substrate

Neutron reflectometry (NR) studies

Even more relevant for our scientific question than the structural evolution in solution is the change that takes place directly at the interface between liquid and solid. Therefore, NR experiments were done to understand better the adsorption behavior of surfactants on a hydrophilized solid silicon substrate. The water contact angle on bare silicon is reported to be 47 º, whereas that after RCA treatment is reported to be less than 5º.[31,32] Based on our research the contact angle on the human arm skin is between 50 and 60º before washing arms with soaps. Therefore, the hydrophilized Si wafer is somewhat more hydrophilic than the skin, but overall reasonable as a model system. In addition, it is well known that phospholipids can form bilayer on hydrophilized silica.[33] Figure 6 shows the neutron reflectometry data of D_2O/glycerol/EO30PS solutions at 25 °C.

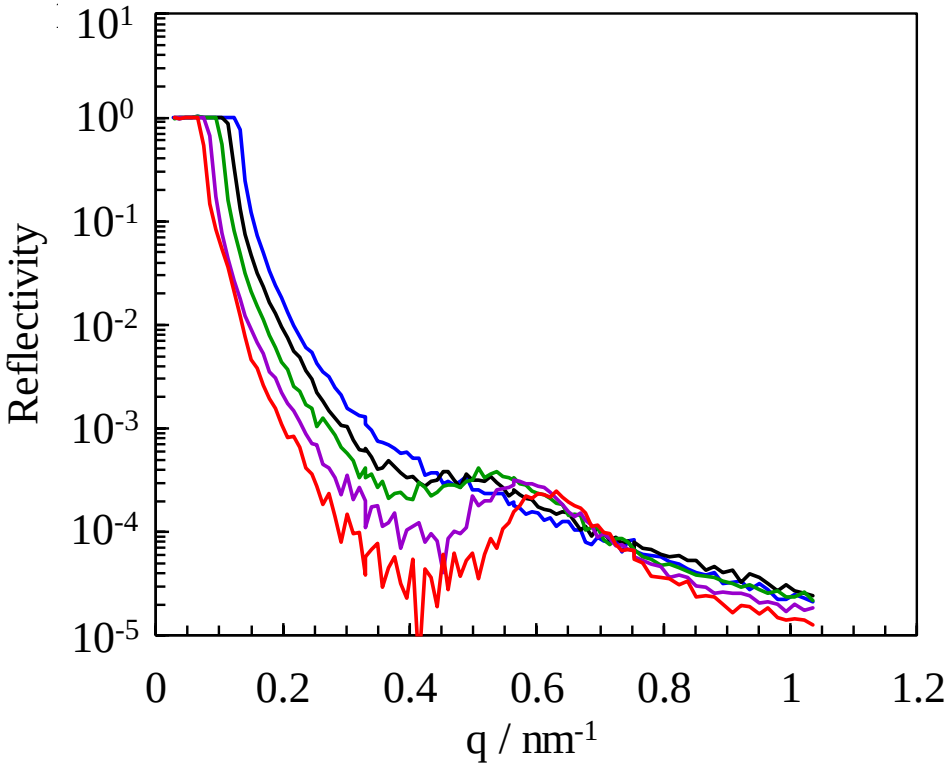

Figure 6. Neutron reflectometry data of D_2O/glycerol/EO30PS solutions at 25 °C: D_2O/glycerol/EO30PS = 85.5/9.5/5 (blue), 72/18/10 (black), 59.5/25.5/15 (green), 48/32/20 (purple), and 37.5/37.5/25 (red). Sample compositions are based on light water.

Generally, the higher the concentration of EO30PS, the better the contrast perpendicular to the surface because the amount of deuterated material at the interface should decrease. With increasing EO30PS concentration, the slope of the reflectivity curves increases, thereby indicating that the amount of deposited hydrogenated material on the Si-wafer increases. At the same time the peaks became more pronounced, which indicates that the degree of ordering was becoming higher, and the peak position shifted to higher q. Peak positions of SANS and NR curves for water/glycerol/EO30PS = 48/32/20 (37.5/37.5/25) system were 0.611 and 0.564 nm^{-1} (0.646 and 0.631 nm^{-1}), respectively. This indicates that the structural dimensions of the self-assembled structures of EO30PS molecules are quite similar in bulk and on a Si wafer, being somewhat larger on the interface and becoming almost identical at high concentrations.

EO30PS molecules do not form bilayers in the bulk solution, but from simple reasoning, the structure of the surfactant layer adsorbed on the substrate can be assumed to consist of at least a bilayer of

EO30PS molecules. For a comparison though cetyl trimethyl ammonium bromide (CTAB) does not form bilayers in the bulk at ambient temperature, as observed here and in previous work for EO30PS,[34-37] it has been reported that CTAB molecules adsorb onto silica in some sort of bilayer structure but not in a uniform fashion.[38-40] In a similar direction, McDermott et al. have studied the adsorption of hexaethylene glycol monododecyl ether ($C_{12}E_6$) on silica or Si/SiO_2 substrate by using NR.[41] They reported that $C_{12}E_6$ molecules adsorb onto silica substrates as a bilayer and that the hydrophilic polyoxyethylene unit, is directed toward the substrate. Our obtained NR curves are very close in appearance to the ones reported by McDermott.

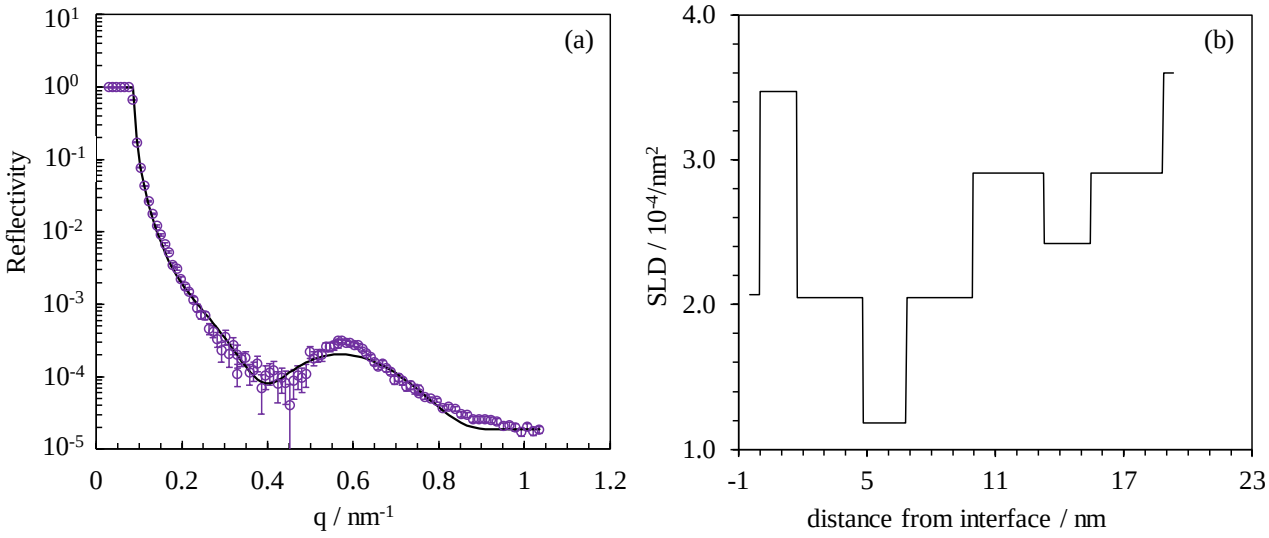

Figure 7. (a) Comparison of the experimental (open circles) and fitting (solid line) neutron reflectivity curves for D_2O/glycerol/EO30PS = 48/32/20 system. (b) SLD profile resulting from the fit.

A first point to be clarified in our analysis is whether the peak seen in the reflectometry curves could not result from bulk scattering. However, a simulation of its effect, using the SANS measurements done on the same sample, shown in Figure S12, demonstrates that not only the peak position is somewhat displaced but especially the SANS peak would not account for the experimentally observed NR intensity. Hence, one can rule out that one sees here bulk scattering and that this is truly adsorption of an ordered structure at the interface. Based on this and taking into account the molecular structure of EO30PS, we obtained a fitting curve and the relevant SLD profile by the fitting as shown in Figure

7 (a) and (b), respectively. The resulting fitting parameters were derived based on Nelson and Prescott[42] analysis and obtained parameters are listed in Table 3. The adsorbed film model of EO30PS molecules on Si wafer is depicted in Figure 8. In our model, we assume that EO30PS molecules form bilayers on the Si substrate, where the hydrophilic group, polyoxyethylene unit, is facing the substrate. With this model and taking into account the molecular constraints, the experimental data of water/glycerol/EO30PS = 48/32/20 were modelled using Motofit[18,19], here allowing some water to penetrate the EO containing layers. For the fitting, we set following constraints. Firstly, the solvent fraction in the first bilayer that is in direct contact with the substrate is less than that in the second bilayer on the first one. Secondly, the length of EO or PS layer was almost the same in each layer. Thirdly, the solvent is located only in the void, which means the volume fraction of EO is the almost the same as that of PS in the respective layer. As conclusion from different fit models, we found that for a reasonable model to describe the overall intensity decrease of the NR curves and the peak seen there, one has to consider two bilayers parallel to the surface. The obtained fit parameters are summarized in Table 3.

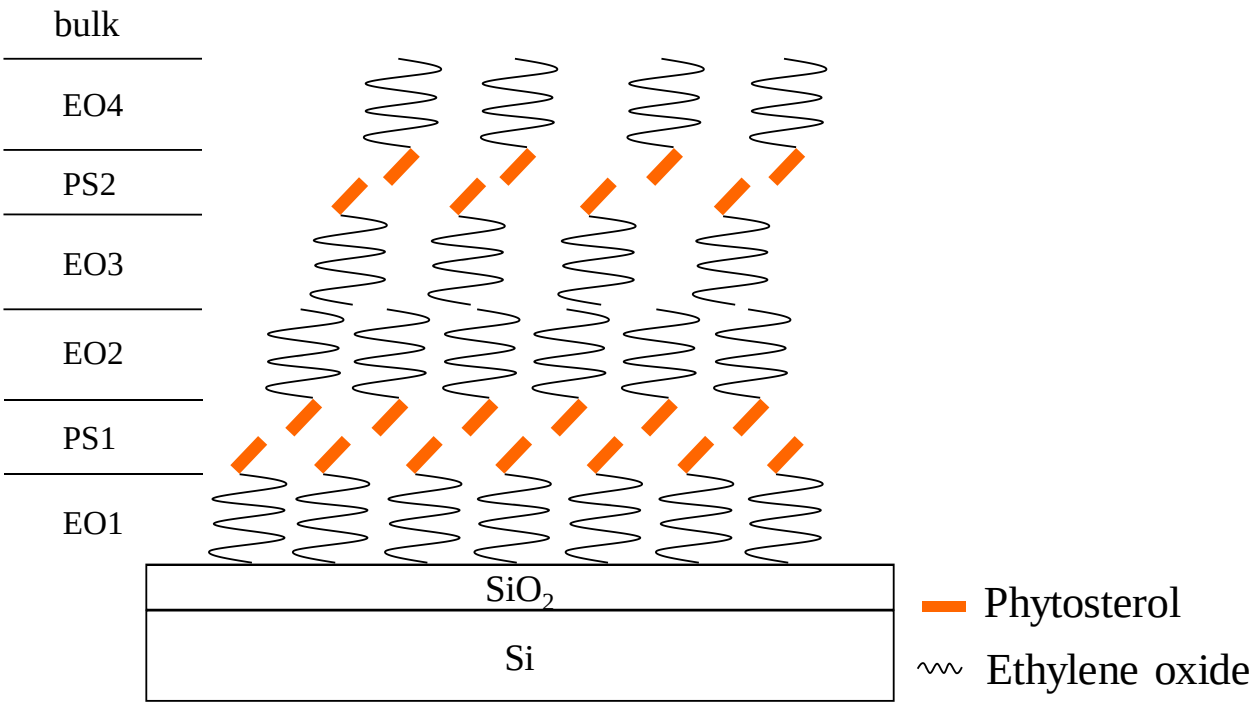

Figure 8. Adsorbed film model for the EO30PS molecules on a Si wafer for D_2O/glycerol/EO30PS = 48/32/20 system.

As a result from the fitting we obtained that the EO layer adsorbed onto the solid substrate has a thickness of 3.1 nm and contains some water that leads to the somewhat higher SLD there (see Table 3). Since the length of the cholesterol molecule is about 1.6 – 1.7 nm,[29] the thickness of the hydrophobic part of a bilayer based on two facing phytosterol units without overlapping would be 3.3 nm. However, experimentally the hydrophobic PS bilayer is only 2.0 nm thick which is much less than this value. This means that one does not have a simple bilayer but this thinning must be the result of a combination of interdigitation and tilting of the molecule. In any case, the much thinner PS part of the bilayer is to be expected from the fact that, as seen from the bulk aggregates, the packing parameter of the EO30PS molecules would favour the formation of rather curved aggregates. At the surface it is apparently forced to pack in bilayers, but for simple geometry reasons then for the given, relatively large head group area, it has to form bilayers with a hydrophobic part that is much thinner than twice the stretched PS chain.

Table 3. Parameters obtained from the NR analysis for D_2O/glycerol/EO30PS = 48/32/20 system (for their meaning refer to Figure 7(b)).

layer	thickness / nm	SLD /10^{-4} nm^{-2}	volume fraction (EO or PS)
Si	Infinite	2.07	-
SiO_2	1.7 ± 0.1	3.47	-
EO1	3.1 ± 0.1	2.05 ± 0.07	0.60 ± 0.02
PS1	2.0 ± 0.1	1.18 ± 0.05	0.72 ± 0.01
EO2	3.1 ± 0.1	2.05 ± 0.03	0.60 ± 0.01
EO3	3.4 ± 0.1	2.91 ± 0.04	0.36 ± 0.01
PS2	2.2 ± 0.2	2.42 ± 0.06	0.42 ± 0.01
EO4	3.4 ± 0.2	2.91 ± 0.04	0.36 ± 0.01
Bulk	Infinite	3.60	-

The second bilayer, needed for describing the NR data is generally a bit thicker and also possesses a higher SLD, indicating a higher water content. Including it into the model then yields a good description of the experimental data, as seen in Figure 7(a). Apparently, the first bilayer, that is in direct contact with the substrate, is covered by a second bilayer, separated by a layer of 6.5 nm (EO2 and EO3 in Figure 8, and Table 3) of solvent and EO30 chains. The theoretical scattering length

densities (SLDs) for pure polyoxyethylene (EO30), phytosterol (PS), and solution (the backing) are 0.72, 0.06, and 3.60 10^{-4}/nm^2, respectively. This means that compared to the experimental data, the EO part directly on the substrate should be substantially solvated and in this model it contains 40% solvent. The solvent fraction (D_2O + glycerol) increases from the first bilayer to the second bilayer up to 64% under the presumption that the hydrophilic material (D_2O/glycerol/EO30) is distributed homogenously within each slab. The obtained thickness of the EO slabs of 3.1 and 3.4 nm appears to be realistic for an EO30 chain, especially when considering that in the range between the bilayers also some interdigitation of the EO chains can easily take place.

This interpretation can be compared to recent papers, where Griffin et al. have reported that three or four condensed bilayers of calcium Aerosol-OT were adsorbed onto mica,[43] and Thomas et al. observed the multilayering phenomena at the air/water interface by using NR.[44] Therefore one can conclude that EO30PS molecules may also form bilayers on the Si/SiO_2 surface though they cannot form in the bulk. Since geometrically the maximum length of an EO unit is between 0.28 and 0.30 nm,[45-47] the length of 30 EO units should be 8.4~9.0 nm if fully stretched. Fick et al. have reported that the length of an EO unit is 0.28 nm in a helical and 0.36 nm in an all-trans conformation and that the film thickness of 45 EO (polyoxyethylene 45) units increased from 2.5 nm in the dry state to 7.0 nm in contact with D_2O (which is much less than the fully stretched chain).[48] Based on their results, the film thickness of 30 EO units should be from 1.7 nm in the dry state to 4.7 nm in contact with D_2O. The length obtained from fitting as shown in Figure 7 was 3.5 nm, which is a little smaller than the fully hydrated state probably due to the presence of glycerol. Related observations were done by Lindman et al., who studied the structure of micellar solutions $C_{12}EO_8$ using Nuclear Magnetic Resonance (NMR).[49] According to them, the EO chains are far from an extended configuration and the experimental average length of the ethylene oxide chain in the micelle would be lower than 1.4 nm, which means 0.18 nm per EO unit. Magid et al. evaluated the micelle structure of $C_{12}EO_8$ using SANS and reported that the length of the ethylene oxide chain was between 1.7 and 1.8 nm, which means between 0.21 and 0.23 nm per EO unit.[50] Our obtained result is still a little smaller than their

results, however, this can be explained by the fact that the molecules are tilted by ~45°, thereby leading to a simultaneous thinning of the hydrophobic and hydrophilic part of the bilayer.

In summary, it can be stated that our model depicted in Figure 8 with the parameters summarized in Table 3 gives not only a good description of the experimental data, but also is a realistic model for the molecular conditions at the interface. The finding of the formation of a double bilayer under these conditions is a bit surprising for this surfactant with a rather large hydrophilic head group, but apparently the self-assembly process taking place at high concentration and rather high glycerol content in the solvent dominates under these conditions the self-assembly process. Certainly here the interaction with the substrate and the head groups must play a major role. However, the Si-OH groups of the substrate should be able to form effective H-bonds with the EO units and in general EO is known to interact attractively with silica. Such an attractive interaction will reduce the hydration of the head groups of the EO30PS and its attraction to the surface thus explains the shape transition from ellipsoidal micelles to bilayers.

4. *CONCLUSIONS*

In this study we investigated the self-assembled structures in bulk and on a hydrophilic substrate (with a similar contact angle for water as skin) for a nonionic surfactant, polyoxyethylene (30) phytosteryl ether (EO30PS), as a function of total concentration and the glycerol/water ratio, which acted as a mixed solvent here. This ternary system is a model system for a real skin lotion and the investigated changes were to mimic the changes occurring during the drying process of such a lotion on skin. For the bulk, SANS measurements revealed that EO30PS micelles simply pack more densely during the drying process (it might be noted that we did not perform an actual drying of the system, but prepared individual samples that would correspond to such a drying process) but do not change much their ellipsoidal shape. On the other hand, EO30PS molecules form double bilayers on the Si/SiO_2 surface at higher concentration. This substantial change of shape of the aggregation state is induced by the surface, but requires a substantial change of the packing conditions. For a given constant head group

area (and thereby constant packing parameter[51]) of the surfactant, they have to be tilted in these bilayers and/or one has to have substantial interdigitation of the respective monolayers forming the bilayer. This mismatch to the packing parameter of the EO30PS molecule then might also explain, why even at rather high concentrations, no more than two bilayers are observed at the surface, as in principle the EO30PS does not want to form flat aggregates and they are only induced due to the interaction with the surface. Here, it should also be noted that these experiments were done at rather high glycerol content, as realistically being the case during a drying process, where the EO30 head group becomes increasingly less solvated, thereby forming a rather compact head group that will attractively interact with the one of the neighboring bilayer.

Our results demonstrate that the self-assembled structure formed on the substrate at higher concentrations is substantially different from that in bulk. EO30PS molecules do form bilayers (but no further extended layering is seen) on the Si/SiO_2 surface, although they form globular micelles in the bulk, a behavior as similarly seen for CTAB molecules[37-39], where time-resolved AFM measurements have even allowed to follow their formation directly.[52] This is an important finding for developing further such surfactant-based systems as formulations for skin care, since the relation between the bulk formulation and the behavior at the interface is essential for a proper scientific understanding. And this surface enforced formation of bilayers will have a substantial impact on the delivery properties from the lotion to the skin, as here now two perpendicular bilayers have to be crossed.

Supporting Information

The Supporting Information is available free of charge at https://pubs.acs.org/doi/10.1021/???.

micrographs from polarization microscopy, DLS autocorrelation functions with cumulant fits, details of SANS analysis, neutron reflectometry.

NOTES

The authors declare there are no conflicts of interest.

Acknowledgements

SANS measurements were performed at the spectrometer PAXY in Laboratoire Léon Brillouin (LLB), France (Experiment No. 12634). NR measurements were performed at V6 (16204613-ST and 17105281-ST) in Helmholtz-Zentrum Berlin (HZB), Germany. For allocation of beamtime we would like to thank the LLB and the HZB.

5. *References*

(1) Magdassi, S. Delivery systems in cosmetics. *Coll. Surfaces A* **1997**, *123−124*, 671−679.

(2) Mihranyan, A.; Ferraz, N.; Stromme, M. Current status and future prospects of nanotechnology in cosmetics. *Prog. Mat. Sci.* **2012**, *57*, 875−910.

(3) van der Kooij, H. M.; Fokkink, R.; van der Gucht, J.; Sprakel. J. Quantitative imaging of heterogeneous dynamics in drying and aging paints. *Sci. Rep.* **2016**, *6*, 34383

(4) Tadros, T. F. Colloids in Cosmetics and Personal Care, *Wiley,* **2008,** *4*.

(5) Ferretti, G. L.; Cabral, J. T. Phase behaviour and non-monotonic film drying kinetics of aluminium chlorohydrate-glycerol-water ternary solutions. *J. Colloid Interface Sci.* **2016,** *481*, 263−270.

(6) Zamlynny, V.; Burgess, I.; Szymanski, G.; Lipkowski, J.; Majewski, J.; Smith, G.; Satija, S.; Ivkov, R. Electrochemical and neutron reflectivity studies of spontaneously formed amphiphilic surfactant bilayers at the gold-solution interface. *Langmuir* **2000,** *16*, 9861−9870.

(7) Berne, B. J.; Pecora, R. Dynamic Light Scattering: With Applications to Chemistry, Biology and Physics, reprint ed.; Dover Publications: Mineola, NY, **2000**.

(8) Hoffmann, I.; Heunemann, P.; Prevost, S.; Schweins, R.; Wagner, N. J.; Gradzielski, M. Self-aggregation of mixtures of oppositely charged polyelectrolytes and surfactants studied by rheology, dynamic light scattering and small-angle neutron scattering. *Langmuir* **2011,** *27*, 4386−4396.

(9) Koppel, D. E. Analysis of Macromolecular Polydispersity in Intensity Correlation Spectroscopy: The Method of Cumulants. *J. Chem. Phys.* **1972,** *57*, 4814−4820.

(10) Chen, S.H.; Lin T.L. 1987 *Methods of Experimental Physics: Neutron Scattering*, ed Price, D.L and Sköld, K (San Diego, CA: Academic) **1987**, *23*, 489–543.

(11) Zemb, T. Lindner, P. Neutron, X-rays and light. Scattering methods applied to soft condensed matter. *Elsevier* 1988.

(12) Keiderling, U. The New BerSANS-PC Software for Reduction and Treatment of Small Angle Neutron Scattering Data. *Appl. Phys. A: Mater. Sci. Process.* **2002**, *74*, s1455−s1457.

(13) Evers, F.; Steitz, R.; Tolan, M.; Czeslik, C. Analysis of Hofmeister effects on the density profile of protein adsorbates: a neutron reflectivity study. *J. Phys. Chem. B* **2009**, *113*, 8462−8465.

(14) Wood, M. H.; M.T. Casford, M. T.; Steitz, R.; Zarbakhsh, A.; Welbourn, R. J. L.; Clarke, S. M.

Comparative adsorption of saturated and unsaturated fatty acids at the iron oxide/oil interface. *Langmuir* **2016,** *32*, 543−540.
(15) Jerliu, B.; Hüger, E.; Dörrer, L.; Seidlhofer, B. K.; Steitz, R.; Oberst, V.; Geckle, U.; M. Bruns, M.; Schmidt, H. Volume expansion during lithiation of amorphous silicon thin film electrodes studied by in-operando neutron reflectometry. *J. Phys. Chem. C* **2014,** *118*, 9395−9399.
(16) Steitz, R.; Braun, C.; Bowers, J.; Lang, P.; Findenegg, G.H. Surface effects accompanying the Lα-to-Lα+ transition of the amphiphile C12E4 in water as studied by neutron reflectivity. *Ber. Bunsenges. Phys. Chem.* **1998,** *102*, 1615−1619.
(17) Kern, W. The evolution of silicon wafer cleaning technology. *J. Electrochem. Soc.* **1990,** *137*, 1887−1892.
(18) Nelson, A. Motofit − Integrating Neutron Reflectometry Acquisition, Reduction and Analysis into One, Easy to Use, Package. *J. Phys.: Conf. Ser.* **2010**, *251*, 012094.
(19) Nelson, A. Co-refinement of multiple-contrast neutron/X-ray reflectivity data usingMOTOFIT. *J. Appl. Crystallogr*. **2006**, *39*, 273−276.
(20) Folmer, B. M.; Svensson, M.; Holmberg, K.; Brown, W. The physicochemical behavior of phytosterol ethoxylates. *J. Colloid Interface Sci.* **1999**, *213*, 112−120.
(21) Fontell, K. Cubic Phases in surfactant and surfactant-like lipid systems. *Coll. Polym. Sci.* **1990**, *268*, 264−285.
(22) Gradzielski, M.; Hoffmann, H.; Panitz, J.-C.; Wokaun, A. Investigations on L2-Phase and Cubic Phase in the System AOT/1-Octanol/Water. *J. Colloid Interface Sci.* **1995**, *169*, 103−118.
(23) Gradzielski, M.; Hoffmann, H.; Oetter, G. Ringing Gels: Their Structure and Macroscopic Properties. *Colloid Polym. Sci.* **1990**, *268*, 167−178.
(24) Naito, N.; Acharya, D. P.; Tanimura, J.; Kunieda, H. Phase behavior of polyoxyethylene phytosterol / polyoxyethylene dodecylether / water systems. *J. Oleo Sci.* **2005**, *54*, 7−13.
(25) Teshigawara, T.; Miyahara, R.; Fukuhara, T.; Oka, T. Development of novel cosmetic base using sterol surfactant. II. Solubilizing of sparingly soluble ultraviolet ray absorbers. *J. Oleo Sci.* **2009**, *58*, 27−36.
(26) Sheely, M. L.; Works, A. M. Glycerol viscosity tables. *Ind. Eng. Chem.* **1932,** *24*, 1060−1064.
(27) Segur, J. B.; Oberstar, H. E. Viscosity of glycerol and its aqueous solutions. *Ind.Eng.Chem.* **1951,** *43*, 2117−2120.
(28) Hoyt, L. F. New table of the refractive index of pure glycerol at 20 ºC. *Ind. Eng. Chem.* **1934,** *26*, 329−332.
(29) Hofsäß, C.; Lindahl, E.; Edholm, O. Molecular dynamics simulations of phospholipid bilayers with cholesterol. *Biophys. J.* **2003**, *84*, 2192−2206.
(30) Iwanaga, T.; Suzuki, M.; Kunieda, H. Effect of added salts or polyols on the liquid crystalline structures of polyoxyethylene-type nonionic surfactants. *Langmuir* **1998,** *14*, 5775−5781.
(31) Krishnaswamy, R.; Ghosh, S. K.; Lakshmanan, S.; Raghunathan, V. A.; Sood, A. K. Phase behavior of concentrated aqueous solutions of cetyltrimethylammonium bromide (CTAB) and sodium hydroxy naphthoate (SHN). *Langmuir* **2005,** *21*, 10439−10443.

(32) Moore, E.; Delalat, B.; Vasani, R.; McPhee, G.; Thissen, H.; Voelcker, N. H. Surface-initiated hyperbranched polyglycerol as an ultralow-fouling coating on glass, silicon, and porous silicon substrates. *ACS Appl. Mater. Interfaces* **2014,** *6*, 15243−15252.
(33) Wang, J.; Zhu, T.; Song, J.; Liu, Z. Gold nanoparticulate film bound to silicon surface with self-assembled monolayers. *Thin Solid Films* **1998,** *327−329*, 591−594.
(34) Kreuzer, M.; Kaltofen, T.; Steitz, R.; Zehnder, B. H.; Dahint, R. Pressure cell for investigations of solid−liquid interfaces by neutron reflectivity. *Rev. Sci. Instrum.* **2011,** *82*, 023902.
(35) Auvray, X.; Petipas, C.; Anthore, R.; Rico, I.; Lattes, A. X-ray diffraction study of mesophases of cetyltrimethylammonium bromide in water, formamlde, and glycerol. *J. Phys.Chem.* **1989**, *93*, 7458−7464.
(36) Coppola, L.; Gianferri, R.; Nicotera, I.; Oliviero, C.; Ranieri, G. A. Structural changes in CTAB/H_2O mixtures using a rheological approach. *Phys. Chem. Chem. Phys.* **2004**, *6*, 2364−2372.
(37) Montalvo, G.; Valiente, M.; Rodenas, E. Study of the phase diagram of the CTAB/Benzyl alcohol/water system. *J. Colloid Interface Sci.* **1995**, *172*, 494−501.
(38) Rennie, A. R.; Lee, E. M.; Simister, E. A.; Thomas, R. K. Structure of a cationic surfactant layer at the silica-water interface. *Langmuir* **1990,** *6*, 1031−1034.
(39) Söderlind, E.; Stilbs, P. A ^{2}H NMR study of two cationic surfactants adsorbed on silica particles. *Langmuir* **1993,** *9*, 2024−2034.
(40) Fragneto, G.; Thomas, R. K.; Rennie, A. R.; Penfold, J. Neutron reflection from hexadecyltrimethylammonium bromide adsorbed on smooth and rough silicon surfaces. *Langmuir* **1996,** *12*, 6036−6034.
(41) McDermott, D. C.; Lu, J. R.; Lee, E. M.; Thomas, R. K. Study of the adsorption from aqueous solution of hexaethylene glycol monododecyl ether on silica substrates using the technique of neutron reflection. *Langmuir* **1992,** *8*, 1204−1210.
(42) Nelson, A. R. J.; Prescott, S. W. Refnx: neutron and X-ray reflectometry analysis in Python. *J. Appl. Cryst.* **2019,** *52*, 193−200.
(43) Griffin, L. R.; Browning, K. L.; Lee, S. Y.; Skoda, M. W. A.; Rogers, S.; Clarke, S. M. Multilayering of calcium aerosol-OT at the mica/water interface studied with neutron reflection: formation of a condensed lamellar phase at the CMC. *Langmuir* **2016,** *32*, 13054−13064.
(44) Thomas, R. K.; Penfold, J. Multilayering of surfactant systems at the air−dilute aqueous solution interface. *Langmuir* **2015,** *31*, 7440−7456.
(45) Vanderah, D. J.; Parr, T.; Silin, V.; Meuse, C. W.; Gates, R. S.; La, H.; Valindius, G. Isostructural self-assembled monolayers. 2. methyl 1-(3-mercaptopropyl)-oligo(ethylene oxide)s. *Langmuir* **2004,** *20*, 1311−1316.
(46) Takahashi, Y.; Tadokoro, H. Structural Studies of Polyethers, (-(CHz) *m-O-)n.* X. Crystal Structure of Poly(ethy1ene oxide). *Macromolecules* **1973**, *23*, 672−675.
(47) Kobayashi, M.; Sakashita, M. Morphology dependent anomalous frequency shifts of infrared absorption bands of polymer crystals: Interpretation in terms of transition dipole-dipole coupling theory. *J. Chem. Phys.* **1992**, *96*, 748−760.

(48) Fick, J.; Steitz, R.; Leiner, V.; Tokumitsu, S.; Himmelhaus, M.; Grunze, M. Swelling behavior of self-assembled monolayers of alkanethiol-terminated poly(ethylene glycol): a neutron reflectometry study. *Langmuir* **2004,** *20*, 3848−3853.
(49) Nilsson, P-G.; Wennerström, H.; Lindman, B. Structure of micellar solutions of nonionic surfactants. Nuclear Magnetic Resonance self-diffusion and proton relaxation studies of poly (ethylene oxide) alkyl ethers. *J. Chem. Phys.* **1983**, *87*, 1377−1385.
(50) Magid, L. J.; Triolo, R.; Johnson, J. S. Small-angle neutron-scattering study of critical phenomena in aqueous solutions of C12E8, a nonionic amphiphile. *J. Chem. Phys.* **1984**, *88*, 5730−5734.
(51) Israelachvili, J. N.; Mitchell, D. J.; Ninham, B. W. Theory of self-assembly of hydrocarbon amphiphiles into micelles and bilayers. *J. Chem. Soc., Faraday Trans. 2*, **1976,** *72*, 1525−1568.
(52) Inoue, S.; Uchihashi, T.; Yamamoto, D.; Ando, T. Direct observation of surfactant aggregate behavior on a mica surface using high-speed atomic force microscopy. *Chem. Commun*. **2011**, *47*, 4974–4976

Table of contents